Curvature and torsion effects in spin-current driven domain wall motion

Kostiantyn V. Yershov,[1,2,*] Volodymyr P. Kravchuk,[1,†] Denis D. Sheka,[3,‡] and Yuri Gaididei[1,§]

[1]*Bogolyubov Institute for Theoretical Physics of National Academy of Sciences of Ukraine, 03680 Kyiv, Ukraine*

[2]*National University of "Kyiv-Mohyla Academy", 04655 Kyiv, Ukraine*

[3]*Taras Shevchenko National University of Kyiv, 01601 Kyiv, Ukraine*

(Received 18 December 2015; revised manuscript received 7 February 2016; published 15 March 2016)

The domain wall motion along a helix-shaped nanowire is studied for the case of spin-current driving via the Zhang-Li mechanism. The analysis is based on the collective variable approach. Two effects are ascertained: (i) the curvature results in the appearance of the Walker limit for a uniaxial wire, and (ii) the torsion results in effective shift of the nonadiabatic spin torque parameter β. The latter effect changes considerably the domain wall velocity and can result in negative domain wall mobility. This effect can be also used for an experimental determination of the nonadiabatic parameter β and damping coefficient α.

DOI: 10.1103/PhysRevB.93.094418

I. INTRODUCTION

The Walker limit [1–3] is a well known property of a one-dimensional domain wall motion in a biaxial magnet. This phenomenon establishes the existence of a critical value f_c of a driving force (e.g., applied magnetic field [1–5] or spin-polarized current [3,5–7]), which corresponds to the bifurcation [5] between two different regimes of the domain wall motion: traveling-wave motion for $f < f_c$ and precession regime for $f > f_c$. The precession regime is characterized by precession of the domain wall magnetization around the wire. In this regime the translation motion of the domain wall along the wire is an oscillating one for a biaxial magnet [2]; however in the limit case of the uniaxial magnet the translational motion becomes stationary [8]. Transition to the precession regime is usually characterized by the rapid decrease (breakdown) of the averaged domain wall velocity (however, the rapid increase is also possible, e.g., for the case of spin-current driving with small nonadiabaticity [6,9,10]).

The critical value f_c is linearly proportional to the coefficient of the transversal anisotropy [1,2] and, therefore, $f_c = 0$ for a uniaxial magnet; this means that the traveling-wave motion is not possible in this case and the precession regime appears for any value of $f > 0$. The *first aim* of the current study is to demonstrate that the domain wall motion in uniaxial curvilinear wire possesses the bifurcation picture with the critical value $f_c \propto \kappa > 0$ with κ being the geometrical curvature of the wire. This effect originates from the curvature-induced effective Dzyaloshinskii-Moriya interaction (DMI) [11].

For the case of spin-current driving via the Zhang-Li mechanism the parameter of the spin-torque nonadiabaticity [12] β is fundamentally important. It is well known [3,5–7,10,12] that for the case $\beta = 0$ a domain wall does not move [13] when $f < f_c$; i.e., the traveling-wave motion is not possible. The *second aim* of the current study is to demonstrate that for the case of a curvilinear wire the nonadiabaticity parameter effectively experiences a geometrically induced shift $\beta \to \beta - \beta^\star$ with $\beta^\star \propto \tau$ with τ being the geometrical torsion of the wire. This effect originates from torsion-induced effective DMI [11]. It can result in negative effective nonadiabaticity parameter and in this case the domain wall demonstrates negative mobility; i.e., it moves against the electron flow. In a particular purely adiabatic case $\beta = 0$ domain walls demonstrate nonzero mobilities; moreover the mobility sign is determined by the product of the helix chirality and domain wall topological charge (head-to-head or tail-to-tail). These phenomena are not observed for a rectilinear wire. However, for a helix nanowire similar behavior of the mobility was recently demonstrated for the Rashba torque driven domain wall motion [14]. In some respects, the effect of chirality-sensitive domain wall mobility is similar to the recently found chiral effects in helical molecules, e.g., the chiral-induced spin selectivity effect in helical molecules [15–17] and magnetochiral dichroism [18,19].

The paper is organized as follows: In Sec. II we introduce basic geometrical notations and parametrization of a helix wire; in Sec. III we demonstrate how the basic equations of motion with the corresponding Lagrange formalization are modified due to the curvature and torsion; in Sec. IV we apply the collective variable approach in order to study static and dynamic properties of the domain wall; the main results are summarized in Sec. V; in Appendix A the details of the collective variable approach are presented; bifurcation analysis of the domain wall dynamics is performed in Appendix B; in Appendix C we present details of numerical simulations.

II. FORMALIZATION OF GEOMETRY

To determine the role of curvature and torsion in the domain wall dynamics we consider a wire in form of a three-dimensional helix as a case study. In this case the geometrical effects are the most demonstrable due to constant curvature and torsion. It is important to note that magnetic microhelices were recently produced experimentally [20,21].

We parametrize the helix curve $\boldsymbol{\gamma}(s)$ in the following way:

$$\boldsymbol{\gamma}(s) = \mathcal{R}\left[\boldsymbol{e}_x \cos\frac{2\pi s}{s_0} + \boldsymbol{e}_y \sin\frac{2\pi s}{s_0}\right] + \boldsymbol{e}_z \mathcal{C}\frac{s}{s_0}\mathcal{P}, \quad (1)$$

*yershov@bitp.kiev.ua
†vkravchuk@bitp.kiev.ua
‡sheka@univ.net.ua
§ybg@bitp.kiev.ua

where s is a natural parameter (arc length), $(\boldsymbol{e}_x,\boldsymbol{e}_y,\boldsymbol{e}_z)$ is a Cartesian basis, $\mathcal{R}$ and $\mathcal{P}$ are radius and pitch of the helix, respectively, and $\mathcal{C}=\pm1$ is the helix chirality, right ($\mathcal{C}=+1$) or left ($\mathcal{C}=-1$). Parameter $s_0=\sqrt{\mathcal{P}^2+4\pi^2\mathcal{R}^2}$ is the length of a single helix coil. However, the Cartesian reference frame is not convenient for a curvilinear wire; therefore in the following we proceed to the local Frenet-Serret reference frame, described by the curvilinear basis vectors $(\boldsymbol{e}_\mathrm{T},\boldsymbol{e}_\mathrm{N},\boldsymbol{e}_\mathrm{B})$ with $\boldsymbol{e}_\mathrm{T}=\boldsymbol{\gamma}'(s)$, $\boldsymbol{e}_\mathrm{N}=\boldsymbol{\gamma}''(s)/|\boldsymbol{\gamma}''(s)|$, and $\boldsymbol{e}_\mathrm{B}=\boldsymbol{e}_\mathrm{T}\times\boldsymbol{e}_\mathrm{N}$ being the tangential, normal, and binormal unit vectors, respectively. Here and below the prime denotes the derivative with respect to the arc length coordinate s. In contrast to the Cartesian basis the local basis is spatially dependent and its differential properties are determined by the Frenet-Serret formulas

$$\boldsymbol{e}_\mathrm{T}'(s)=\kappa\boldsymbol{e}_\mathrm{N},\quad \boldsymbol{e}_\mathrm{N}'(s)=-\kappa\boldsymbol{e}_\mathrm{T}+\tau\boldsymbol{e}_\mathrm{B},\quad \boldsymbol{e}_\mathrm{B}'(s)=-\tau\boldsymbol{e}_\mathrm{N}. \tag{2}$$

One can consider (2) as a definition of curvature κ and torsion τ of the wire. A helix curve has a specific feature: the curvature $\kappa=4\pi^2\mathcal{R}/s_0^2$ as well as the torsion $\tau=2\pi\mathcal{C}\mathcal{P}/s_0^2$ are constants. By setting values of both parameters κ and τ (with sign) one determines the helix curve in unique way; thus, in the following discussion we use κ and τ as only geometrical parameters.

In order to consider a physical wire of finite thickness, one can use the following parametrization:

$$\boldsymbol{r}(s,\chi,\rho)=\boldsymbol{\gamma}(s)+\rho\cos\chi\,\boldsymbol{e}_\mathrm{N}(s)+\rho\sin\chi\,\boldsymbol{e}_\mathrm{B}(s). \tag{3}$$

Here the three-dimensional radius vector $\boldsymbol{r}$ defines the space domain, occupied by the wire; $\rho\in[0,\rho_0]$ and $\chi\in[0,2\pi)$ are coordinates within the wire cross section with ρ_0 being the wire radius. For an example of a helix wire defined by (3) and (1) see Fig. 1(b).

III. EQUATIONS OF MOTION

By reasons of the nontrivial curvilinear geometry the spin-polarized current is more preferable driving for a domain wall on the helix wire as compared with the external magnetic field. Thus, we base our study on the Landau-Lifshitz-Gilbert equation with additional Zhang-Li spin-torque terms [6,12,22]

$$\dot{\boldsymbol{m}}=\omega_0\boldsymbol{m}\times\frac{\delta\mathcal{E}}{\delta\boldsymbol{m}}+\alpha\boldsymbol{m}\times\dot{\boldsymbol{m}} +\boldsymbol{m}\times[\boldsymbol{m}\times(\boldsymbol{u}\cdot\nabla)\boldsymbol{m}]+\beta\boldsymbol{m}\times(\boldsymbol{u}\cdot\nabla)\boldsymbol{m}. \tag{4}$$

Here $\boldsymbol{m}=\boldsymbol{M}/M_s$ is the unit magnetization vector with M_s being the saturation magnetization. The overdot indicates the derivative with respect to time and the characteristic time scale of the system is determined by $\omega_0=4\pi\gamma_0 M_s$ with γ_0 being the gyromagnetic ratio. Here $\mathcal{E}=E/(4\pi M_s^2)$ is the normalized total energy of the system. The driving strength is presented by the quantity $\boldsymbol{u}=\boldsymbol{j}P\mu_B/(|e|M_s)$ which is close to average electron drift velocity in the presence of the current of density $\boldsymbol{j}\|\boldsymbol{e}_\mathrm{T}$ [23]; here P is the rate of spin polarization, μ_B is the Bohr magneton, and e is electron charge. Constants α and β denote Gilbert damping and the nonadiabatic spin-transfer parameter, respectively.

The simple form of (4) without the nonadiabatic term was first obtained in Ref. [22] within the ballistic transport model for half-metallic materials. Later in Ref. [12] the nonadiabatic spin-transfer term was introduced. For detailed derivation of the spin-torques and applications see reviews Refs. [23–26].

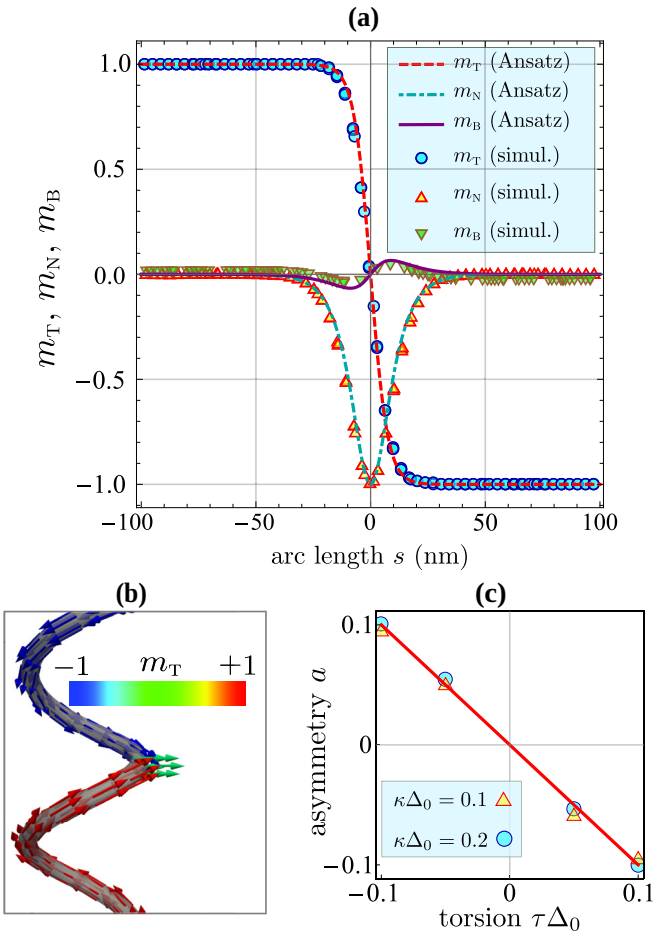

FIG. 1. Static head-to-head ($p=+1$) domain wall on a helix wire with chirality $\mathcal{C}=+1$. (a) Magnetization profiles: markers and lines correspond to micromagnetic simulations and ansatz (10), respectively. Ansatz (10) is utilized with the equilibrium values of parameters (12), where the domain wall width $\Delta_0=2\ell$ corresponds to the magnetically soft material. Helix radius and pitch are $\mathcal{R}=30$ nm and $\mathcal{P}=93$ nm, respectively ($\kappa\Delta_0=0.2$, $\tau\Delta_0=0.1$). For simulation details see Appendix C. (b) Magnetization distribution obtained from the simulations. (c) The domain wall asymmetry parameter a for various torsions and curvatures: symbols correspond to simulations and line shows the dependence $a=-\tau\Delta_0$; see Eq. (12).

To write the energy functional $\mathcal{E}$ we consider a simple magnetic wire model, which takes into account only two contributions to the total magnetic energy:

$$\mathcal{E}=\mathcal{S}\int_{-\infty}^{+\infty}\left[\ell^2\mathcal{E}_\mathrm{ex}-k_\mathrm{t}(\boldsymbol{m}\cdot\boldsymbol{e}_\mathrm{T})^2\right]ds, \tag{5}$$

namely, exchange one $\mathcal{E}_\mathrm{ex}$ and easy-tangential anisotropy—the second term in (5). Here $\mathcal{S}=\pi\rho_0^2$ is area of the wire cross section, $\ell=\sqrt{A/4\pi M_s^2}$ is the exchange length with A being exchange constant, and $k_\mathrm{t}=K/(4\pi M_s^2)+1/4$ is the dimensionless anisotropy constant. Here $K>0$ is an

easy-tangential magnetocrystalline anisotropy constant and the term $1/4$ comes from the magnetostatic contribution [2,27–29]. Recently we demonstrated that model (5) accurately describes dynamics of a transversal domain wall in thin curvilinear wire even for a magnetically soft ($K = 0$) material: for plain wires [30] and microhelix wires [14]. Competition of the exchange and anisotropy contributions results in the length scale of the system $\Delta_0 = \ell/\sqrt{k_t}$. For magnetically soft wires one has $\Delta_0 = 2\ell$. In (5) and everywhere below we restrict ourselves to the case of a thin wire $\rho_0 \lesssim \Delta_0$; this justifies our assumption of one-dimensionality of the problem: magnetization varies only along the wire and it is uniform within a wire cross section.

Up to now the curvilinearity formally does not appear in the problem (4)–(5). However, the spin-polarized current and anisotropy axis are oriented tangentially to the wire. This makes it convenient to describe the magnetization distributions (e.g., domain walls) in terms of the local curvilinear basis:

$$\begin{aligned} \boldsymbol{m} &= m_{\mathrm{T}}\boldsymbol{e}_{\mathrm{T}} + m_{\mathrm{N}}\boldsymbol{e}_{\mathrm{N}} + m_{\mathrm{B}}\boldsymbol{e}_{\mathrm{B}} \\ &= \cos\theta\,\boldsymbol{e}_{\mathrm{T}} + \sin\theta\cos\phi\,\boldsymbol{e}_{\mathrm{N}} + \sin\theta\sin\phi\,\boldsymbol{e}_{\mathrm{B}}, \end{aligned} \tag{6}$$

where an angular representation is introduced to take into account the constraint $|\boldsymbol{m}| = 1$. Here the crucial point is that the curvilinear basis vectors $(\boldsymbol{e}_{\mathrm{T}}, \boldsymbol{e}_{\mathrm{N}}, \boldsymbol{e}_{\mathrm{B}})$ depend on spatial coordinate s. Therefore, all terms in (4) containing spatial derivatives introduce curvature κ and torsion τ into the problem via Frenet-Serret formulas (2). One can treat it as the emergence of new geometrically induced interactions. Thus, the exchange energy density $\mathscr{E}_{\mathrm{ex}}$ in terms of the angular representation has the following form [11]:

$$\begin{aligned} \mathscr{E}_{\mathrm{ex}} &= \mathfrak{A}^2 + \mathfrak{B}^2, \quad \mathfrak{A} = \theta' + \kappa\cos\phi, \\ \mathfrak{B} &= \sin\theta(\phi' + \tau) - \kappa\cos\theta\sin\phi. \end{aligned} \tag{7}$$

In $\mathscr{E}_{\mathrm{ex}}$, terms linear and bilinear with respect to κ and τ can be treated as effective DMI and anisotropy interactions, respectively [11]. Spin torques in (4) contain space derivatives $(\boldsymbol{u}\cdot\nabla)\boldsymbol{m} = u\,\boldsymbol{m}'$. Substituting the angular parametrization (6) into (4) and taking into account Frenet-Serret formulas (2) one obtains the following angular form of the equations of motion:

$$\begin{aligned} -\sin\theta(\dot\theta + u\theta') &= \omega_0\frac{\delta\mathcal{E}}{\delta\phi} + u\kappa\sin\theta\cos\phi \\ &\quad + \alpha\sin^2\theta\dot\phi + u\beta\sin\theta\,\mathfrak{B}, \\ \sin\theta(\dot\phi + u\phi') &= \omega_0\frac{\delta\mathcal{E}}{\delta\theta} + u(\kappa\cos\theta\sin\phi - \tau\sin\theta) \\ &\quad + \alpha\dot\theta + u\beta\,\mathfrak{A}. \end{aligned} \tag{8}$$

Note the correspondence between the nonadiabatic terms in (8) and summands in the exchange energy density (7).

One can easily verify that Eqs. (8) are Lagrange-Rayleigh equations

$$\frac{\delta\mathcal{L}}{\delta\xi_i} - \frac{\mathrm{d}}{\mathrm{d}t}\frac{\delta\mathcal{L}}{\delta\dot\xi_i} = \frac{\delta\mathcal{F}}{\delta\dot\xi_i}, \quad \xi_i \in \{\theta, \phi\},$$

for the Lagrange function

$$\mathcal{L} = -\mathcal{S}\int_{-\infty}^{\infty}\phi\sin\theta(\dot\theta + u\theta')ds - \omega_0\mathcal{E} - \mathcal{E}^u, \tag{9a}$$

$$\mathcal{E}^u = u\mathcal{S}\int_{-\infty}^{\infty}(\kappa\sin\theta\sin\phi + \tau\cos\theta)ds, \tag{9b}$$

and dissipative function $\mathcal{F} = \mathcal{F}^{\mathrm{G}} + \mathcal{F}^u$, consisting of two summands: the "standard" Gilbert dissipative function [31,32]

$$\mathcal{F}^{\mathrm{G}} = \frac{\alpha}{2}\mathcal{S}\int_{-\infty}^{\infty}(\dot\theta^2 + \sin^2\theta\dot\phi^2)ds \tag{9c}$$

and "nonadiabatic" correction

$$\mathcal{F}^u = u\beta\mathcal{S}\int_{-\infty}^{\infty}(\mathfrak{A}\,\dot\theta + \mathfrak{B}\sin\theta\dot\phi)ds. \tag{9d}$$

Treatment of the Landau-Lifshitz equation in terms of the Lagrange formalism was initially proposed by Döring [33]. In order to take into account the adiabatic spin torque ($\beta = 0$) the corresponding modification of the Lagrange function was proposed by Thiaville [9]; see the second summand in the integrand in (9a). In this paper, in order to take into account the curvilinear effects and nonadiabaticity, we modify the energy functional and dissipative function in accordance with (9b) and (9d), respectively.

IV. COLLECTIVE VARIABLES APPROACH

To analyze the domain wall properties we use the collective variable approach [34–36] based on the generalized q-Φ model [37]

$$\theta = 2\arctan e^{p(s-q)/\Delta}, \quad \phi = \Phi + a\frac{s-q}{\Delta}. \tag{10}$$

Here $\{q, \Phi\}$ and $\{\Delta, a\}$ are pairs of time-dependent conjugated collective variables: q and Φ determine the domain wall position and phase (momentum), respectively; Δ and a determine domain wall width and asymmetry of the phase distribution, respectively. Topological charge p determines the domain wall type: head-to-head ($p = +1$) or tail-to-tail ($p = -1$).

Strictly speaking, ansatz (10) does not correspond to the ground states with distance from the domain wall position $|s - q| \gg \Delta$. Indeed, according to Ref. [38] the ground state of a helix wire with easy-tangential anisotropy cannot be strictly tangential: the magnetization vector $\boldsymbol{m}$ deviates from the tangential direction by an angle $\psi \approx \kappa\tau\Delta_0^2$ (for small curvature and torsion). This can be treated as the result of action of an effective geometry induced magnetic field [11], which in the case of a helix is oriented along binormal vector $\boldsymbol{e}_{\mathrm{B}}$. Thus, in order to use ansatz (10) one has to first rotate the basis $(\boldsymbol{e}_{\mathrm{T}}, \boldsymbol{e}_{\mathrm{N}}, \boldsymbol{e}_{\mathrm{B}})$ by an angle ψ around the normal vector $\boldsymbol{e}_{\mathrm{N}}$ [14]. However, by introducing the angular variables (6) in the rotated reference frame one obtains a set of equations of motion which coincide with (8) up to corrections infinitesimal in κ and τ of the second and third order for the energy $\mathcal{E}$ and spin-torque terms, respectively. Therefore in order to describe effects linear in κ and τ the procedure of the basis adjustment [14] is not required. In the following we restrict ourselves to the linear in

κ and τ analysis in order to keep intelligibility of the solution structure.

A. Static solution

Let us first consider the no driving case. Substituting ansatz (10) into energy functional (5) and taking into account (6) and (7) one obtains the following expression for the energy of a static domain wall:

$$\frac{\mathcal{E}}{2\mathcal{S}} \approx \frac{\ell^2}{\Delta}(1+a^2) + k_t\Delta + 2\ell^2\tau a + \ell^2\pi p\kappa\cos\Phi. \quad (11)$$

The energy approximation (11) saves only linear in κ and τ terms in the corresponding equations for the variational parameters, whose equilibrium values read

$$\Delta_0 \approx \ell/\sqrt{k_t}, \quad a_0 \approx -\tau\Delta_0, \quad \cos\Phi_0 = -p. \quad (12)$$

As well as for the case of a planar curvilinear wire [30] the *curvature* fixes the domain wall magnetization in direction $-p\,\boldsymbol{e}_{\mathrm{N}}$; thus the static head-to-head (tail-to-tail) domain wall is always magnetized outward from (inward toward) the helix; see also Fig. 1. This is due to the last term in (11). However, in contrast to the planar case, the new *torsion* induced parameter of the domain wall asymmetry a_0 appears for the three-dimensional wire. It confirms the recent results of Ref. [14]. In rectilinear wires the similar asymmetry in the domain wall structure appears due to the intrinsic DMI [37,39].

The domain wall structure which is determined by ansatz (10) with parameters (12) is compared with the structure of domain walls obtained by means of micromagnetic NMAG simulations [40]; see Fig. 1. We consider four cases of different domain wall charge $p = \pm 1$ and helix chirality $\mathcal{C} = \pm 1$. In all cases the model (10) demonstrates a very good agreement with the simulations data. Signs of the profiles m_{T} and m_{N} are determined by sign of the topological charge p, while the sign of the binormal component m_{B} is determined by the sign of the product $p\mathcal{C}$. Small curvature and torsion have negligible impact on the profiles m_{T} and m_{N}. However amplitude of the binormal component m_{B} is linear with respect to the torsion and it also practically does not depend on the curvature; see Fig. 1(c).

It should be noted that we perform a full-scale micromagnetic simulation with two interactions taken into account, namely exchange and magnetostatic interactions. The obtained conformity with the theory confirms the physical soundness of the model (5) which assumes that the magnetostatic interaction can be reduced to the easy-tangential anisotropy in thin nanowires.

B. Domain wall dynamics

Here we use a common collective variable approach which enables one to proceed from PDEs (8) to a set of ODEs (A3) with respect to the set of collective variables $\{q(t),\Phi(t),\Delta(t),a(t)\}$; for details see Appendix A. The obtained set (A3) is a nonlinear one, and only numerical analysis is possible in general. However, similarly to the case of a rectilinear wire, the two well separated time scales can be distinguished in this system. The dynamics of the pair $\{\Delta, a\}$ is characterized by the typical frequency $\omega \approx 2\omega_0 k_t/c$, where $c = \pi^2/12$, while the upper estimate of typical frequency of the pair $\{q, \Phi\}$ is $\Omega = p(\beta - \beta^\star - \alpha)u/\Delta_0$, where

$$\beta^\star = p\tau\Delta_0;$$

for details see Appendix A. In practice, the time scale separation condition $\omega \gg |\Omega|$, which can be reformulated as

$$\frac{u}{v_0}|\beta - \beta^\star - \alpha| \ll \frac{2}{c}\sqrt{k_t}, \quad (13)$$

is well satisfied due to small values of α, β, and $\beta^\star$. Here and everywhere below we assume that $u > 0$ with no loss of generality, and the notation $v_0 = \ell\omega_0$ is used. Thus, the dynamics of the pair $\{\Delta, a\}$ is much faster than the dynamics of the pair $\{q, \Phi\}$, which in this case can be described by a set of two equations

$$\begin{aligned} \dot{q} - \alpha p\Delta_0\dot{\Phi} &= u - \pi v_0\ell\kappa\sin\Phi, \\ \alpha p\dot{q} + \Delta_0\dot{\Phi} &= up(\beta - \beta^\star), \end{aligned} \quad (14)$$

where we assume that the damping and the nonadiabaticity are low— $\alpha^2 \ll 1$, $\alpha a \ll 1$, and $\beta^2 \ll 1$—and also the curvature is assumed to be small $\kappa\ell \ll 1$. The values of the fast variables are determined by the values of slow ones in the following way:

$$\begin{aligned} \Delta(t) = \Delta[\Phi(t)] &\approx \frac{\ell}{\sqrt{k_t + \frac{u}{v_0}\frac{\pi}{2}\kappa\ell\sin\Phi}}, \\ a(t) = a[\Phi(t)] &\approx -\Delta\tau - p\frac{\pi}{4}\frac{u}{v_0}\frac{\beta\kappa\ell}{k_t}\sin\Phi. \end{aligned} \quad (15)$$

Equation (14) have a traveling-wave solution $q = Vt$ and $\Phi =$ constant, which exists for the case $u < |u_c|$, where

$$u_c \approx v_0\frac{\pi\alpha\kappa\ell}{\alpha - \beta + \beta^\star} \quad (16)$$

is the Walker limit. The corresponding domain wall velocity is

$$V \approx u\frac{\beta - \beta^\star}{\alpha}. \quad (17)$$

The value of the constant domain wall phase Φ is determined by the equation $\sin\Phi = u/u_c$.

Let us estimate the effective mass of the domain wall [33]. To this end we consider a no driving case ($u = 0$) with vanishing damping. In this case a small deviation $\tilde{\Phi} = \Phi - \Phi_0$ of the domain wall phase from its equilibrium value results in the traveling-wave domain wall motion with the velocity $V \approx p\pi v_0\kappa\ell\tilde{\Phi}$. Using the latter relation and energy expression (11) one can estimate energy of the moving domain wall as $E/\mathcal{S} \approx \varepsilon_0 + \mathcal{M}V^2/2$, where ε_0 is energy density of a stationary domain wall and the quantity

$$\mathcal{M} \approx \frac{8M_s^2}{\kappa v_0^2} \quad (18)$$

can be interpreted as an effective mass of the domain wall per unit area. For a permalloy helix with $\mathcal{R} = \mathcal{P} = 1\,\mu$m one obtains $\mathcal{M} \approx 1.2 \times 10^{-24}\,\mathrm{kg/nm^2}$. This value is close to the one obtained experimentally for permalloy nanostripes [41]. An infinite mass which one obtains in the limit case $\kappa \to 0$ corresponds to the case of a rectilinear biaxial wire with

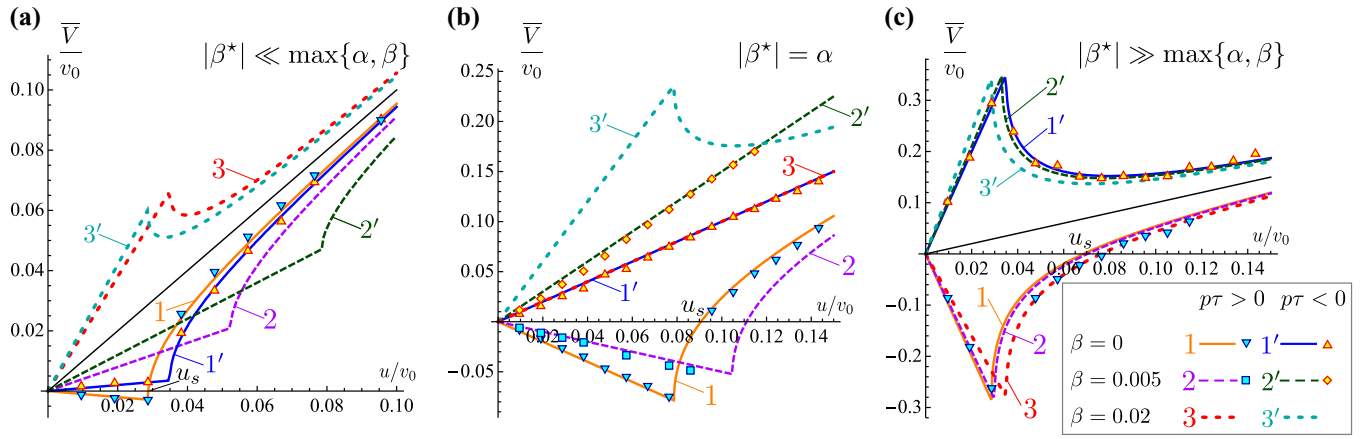

FIG. 2. Averaged domain wall velocity as a function of the applied current. Lines correspond to solutions of the collective variables equations (14), and markers show the results of NMAG micromagnetic simulations. Simulations as well as theoretical solutions are made for magnetically soft wire ($k_t = 1/4$). All the other parameters are as follows: (a) $\kappa\ell = 0.01$, $\tau\ell = 0.0005$ ($|\beta^\star| = 0.001$); (b) $\kappa\ell = 0.05$, $\tau\ell = 0.005$ ($|\beta^\star| = 0.01$); (c) $\kappa\ell = 0.1$, $\tau\ell = 0.05$ ($|\beta^\star| = 0.1$). In all cases $\alpha = 0.01$. The thin solid line corresponds to the case of a rectilinear wire, where $V \approx u$.

vanishing transversal anisotropy [10,33,37,42]. However, in contrast to the case of a rectilinear biaxial magnet, the domain wall mass (18) does not depend on the longitudinal anisotropy k_t. This is because the mass (18) originates mainly from the effective DMI term $\ell^2\pi p\kappa\cos\Phi$ in (11), but not from the anisotropy contribution.

When the applied current achieves the critical value $u = |u_c|$ the system experiences a saddle node bifurcation; see Appendix B for details. When the driving exceeds the critical value $u > |u_c|$ the domain wall demonstrates a precession motion with frequency

$$\Omega_{\text{prec}} = \Omega\sqrt{1 - u_c^2/u^2}; \tag{19}$$

for details see Appendix B. This behavior is typical for the Walker limit overcoming. In the precession regime the domain wall can be characterized by some averaged in time drift velocity $\overline{V}$. Figure 2 demonstrates dependencies $\overline{V}(u)$ for various values of parameters. One can see a typical domain wall behavior with the Walker limit being present. However a few special features should be marked out. A domain wall always moves in the direction of electron flow ($\overline{V} > 0$) for the case $p\tau < 0$, while for the case $p\tau > 0$ it can move in opposite direction. The latter case has two peculiarities: (i) If $\beta \ll |\beta^\star|$ then the traveling-wave motion ($u < u_c$) is always characterized by negative mobility with $V < 0$. (ii) For the precession regime ($u > u_c$) there always is a current value $u_s > u_c$ which corresponds to $\overline{V} = 0$; i.e., the domain wall oscillates around some fixed position. It is important to emphasize that the influence of torsion on the domain wall behavior is determined by the product $p\tau$, so the head-to-head and tail-to-tail domain walls swap roles when the helix chirality (sign of τ) is changed to the opposite one. It also should be noted that the influence of the nonadiabatic parameter β vanishes for the case $|\beta^\star| \gg \max\{\alpha,\beta\}$; see Fig. 2.

Some examples of possible types of the domain wall motions are shown in Fig. 3. One can conclude that the domain wall dynamics in traveling-wave and precession regimes is

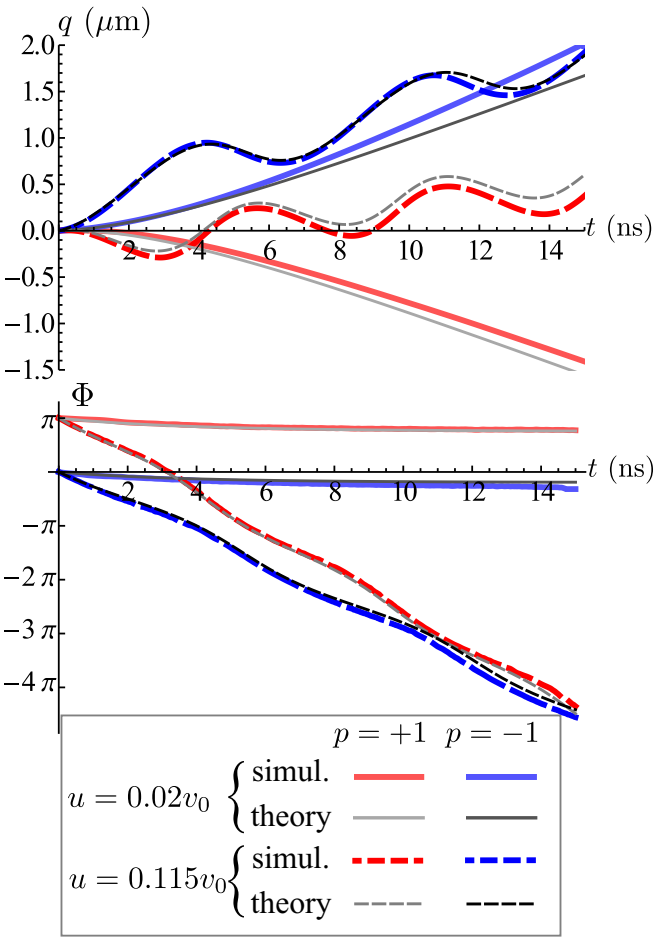

FIG. 3. Different regimes of the domain wall motion in terms of the collective variables. Geometrical parameters of the helix are the same as in Fig. 2(c) and $\beta = 0$. Solid and dashed lines correspond to the traveling-wave ($u = 0.02v_0 < |u_c|$) and precession ($u = 0.115v_0 > |u_c|$) regimes, respectively; the corresponding dynamics is illustrated in the Supplemental Material [43]. Thick and thin lines correspond to simulation data and solutions of Eqs. (14), respectively.

similar to the corresponding domain wall dynamics in a biaxial magnet. One should also note a good correspondence of the simulation data and predictions of the q-Φ model, in spite of the strong simplification (14) of the initial set of equations (A3).

Finally, we would like to note how the result (17) can be used for an experimental estimating of parameters α and β. For this purpose one should measure the domain wall mobility $\mu = V/u$ for two helices with different torsions τ_1 and τ_2 and small curvatures. Then by using (17) and taking into account that $\beta^\star = p\Delta_0\tau$, one obtains the following values of the parameters:

$$\alpha = p\Delta_0\frac{\tau_2-\tau_1}{\mu_1-\mu_2}, \quad \beta = p\Delta_0\frac{\mu_1\tau_2-\mu_2\tau_1}{\mu_1-\mu_2}, \tag{20}$$

where μ_i is the domain wall mobility in the helix with torsion τ_i. However, we are aware that utilizing this method can entail some technical difficulties, e.g., detection of the domain wall position on a three-dimensional wire and pinning of the magnetic domain wall on the wire defects.

V. CONCLUSIONS

The influence of curvature and torsion on the spin-current driven domain wall motion is studied by the example of helical wires. The analytical results are well confirmed by the full-scale micromagnetic simulations. It is shown that the curvature results in the Walker limit appearance (16), while the torsion effectively shifts the material parameter of nonadiabaticity $\beta \to \beta - \beta^\star$, where $\beta^\star = p\tau\Delta_0$; see (14) and the consequences. This effect can lead to a negative effective nonadiabaticity resulting in negative domain wall mobility. Significant influence of the wire torsion on the domain wall motion can be used for an experimental determination of the nonadiabatic parameter β and damping coefficient α; see (20).

Additionally, we show that the effective mass of the domain wall is inversely proportional to the wire curvature. We demonstrate that the Walker limit is a saddle-node bifurcation.

ACKNOWLEDGMENTS

V.K. acknowledges IFW Dresden, where part of this work was performed, for kind hospitality. This work is supported in part by the Alexander von Humboldt Foundation.

APPENDIX A: EQUATIONS OF MOTION FOR COLLECTIVE VARIABLES

Substituting ansatz (10) into (9) and performing integration over s, one obtains the following effective Lagrange function:

$$\mathcal{L} = 2\mathcal{S}p[\Phi(\dot{q}-u) + c\dot{\Delta}a] - \omega_0\mathcal{E} - \mathcal{E}^u, \tag{A1a}$$

where $c = \pi^2/12$, energy $\mathcal{E}$ is determined by (11), and the effective curvature induced spin-torque correction of the energy reads

$$\mathcal{E}^u \approx \mathcal{S}u(\pi\kappa\Delta\sin\Phi + 2p\tau q). \tag{A1b}$$

As follows from (A1), the domain wall asymmetry parameter a is a conjugated momentum to the domain wall width Δ. In the same way one obtains components of the effective dissipative function $\mathcal{F} = \mathcal{F}^{\mathrm{G}} + \mathcal{F}^u$: the Gilbert part

$$\mathcal{F}^{\mathrm{G}} = \frac{\alpha}{\Delta}\mathcal{S}\{\dot{q}^2 + (\dot{q}a - \dot{\Phi}\Delta)^2 + c[\dot{\Delta}^2 + (\dot{a}\Delta - \dot{\Delta}a)^2]\} \tag{A2a}$$

coincides with previously obtained one [37] and the nonadiabatic correction reads

$$\mathcal{F}^u \approx -2u\beta\mathcal{S}\left[\frac{\dot{q}}{\Delta} - \dot{\Phi}(a+\Delta\tau) + p\frac{\pi}{2}\kappa(\dot{q}\cos\Phi - \dot{a}\Delta\sin\Phi)\right]. \tag{A2b}$$

Lagrange function (A1) and dissipative function (A2) generate the following set of equations of motion for the collective variables:

$$(p+\alpha a)\dot{q} - \alpha\Delta\dot{\Phi} = pu\left(1 + p\frac{\pi}{2}\kappa\Delta\cos\Phi\right) - p\pi v_0\ell\kappa\sin\Phi + u\beta(a+\Delta\tau), \tag{A3a}$$

$$\alpha\frac{\dot{q}}{\Delta} + (p-\alpha a)\dot{\Phi} = \frac{u\beta}{\Delta}\left(1 + p\frac{\pi}{2}\kappa\Delta\cos\Phi\right) - pu\tau, \tag{A3b}$$

$$\frac{c}{\omega_0}\left[(p+\alpha a)\frac{\dot{\Delta}}{\Delta} - \alpha\dot{a}\right] = 2\frac{\ell^2}{\Delta^2}(a+\Delta\tau) + p\frac{\pi}{2}\frac{u}{v_0}\beta\kappa\ell\sin\Phi, \tag{A3c}$$

$$\frac{c}{\omega_0}\left[\alpha\frac{\dot{\Delta}}{\Delta} + (p-\alpha a)\dot{a}\right] = \frac{\ell^2}{\Delta^2}(1+a^2) - k_t - \frac{\pi}{2}\frac{u}{v_0}\kappa\ell\sin\Phi, \tag{A3d}$$

where $v_0 = \ell\omega_0$.

First of all, it should be noted that in the no driving case ($u = 0$) Eqs. (A3c) and (A3d) split off the whole set (A3) forming an independent set of equations with respect to Δ and a. The linearization in the vicinity of the stationary point $\{\Delta_0, a_0\}$ with respect to small deviations $\tilde{\Delta} = \Delta - \Delta_0$ and $\tilde{a} = a - a_0$ results in a set of linear equations

$$\begin{Vmatrix} \dot{\tilde{\Delta}}/\Delta_0 \\ \dot{\tilde{a}} \end{Vmatrix} \approx -\frac{2\omega_0}{c}\frac{\ell^2}{\Delta_0^2}\begin{Vmatrix} \alpha-\beta^\star & -p \\ p & \alpha+\beta^\star \end{Vmatrix}\cdot\begin{Vmatrix} \tilde{\Delta}/\Delta_0 \\ \tilde{a} \end{Vmatrix}, \tag{A4}$$

where $\beta^\star = p\Delta_0\tau$. In (A4) the stationary values Δ_0 and a_0 are determined by (12) and the low damping approximation ($\alpha^2 \ll 1, \alpha a_0 \ll 1$) is applied. Equations (A4) have a solution $\tilde{\Delta} = \tilde{\Delta}_0\exp(-\eta t + i\omega t)$ and $\tilde{a} = \tilde{a}_0\exp(-\eta t + i\omega t)$, where

$$\omega \approx \frac{2\omega_0}{c}k_t, \quad \eta = \alpha\omega. \tag{A5}$$

Let us now assume that $\omega \gg \Omega$, where Ω is the characteristic frequency of the pair $\{q, \Phi\}$; i.e., pair $\{\Delta, a\}$ is much faster than the pair $\{q, \Phi\}$. In this case the quasistationary values of Δ and a are slightly modified; see (15).

However the time characteristics of the pair $\{\Delta, a\}$ are the same as (A5). Taking into account (15) one can split off the first two equations of the set (A3) and present them in the form (14).

The characteristic frequency Ω can be easily determined in the case of small curvature. Indeed in the limit case of

vanishing curvature $\kappa \to 0$ and low damping the couple of equations (A3a) and (A3b) take a form

$$p\dot{q} - \alpha\Delta_0\dot{\Phi} = pu, \qquad \alpha\dot{q} + p\Delta_0\dot{\Phi} = u(\beta - \beta^\star), \quad \text{(A6)}$$

which coincides with the well known [6] q-Φ equations for the spin-current driven domain wall motion in a rectilinear uniaxial wire, except for shift of the nonadiabatic parameter $\beta \to \beta - \beta^\star$. Equation (A6) have a solution in the form of uniform domain wall motion $q = Vt$ with uniform phase precession $\Phi = \Omega t$, where

$$V \approx u, \qquad \Omega \approx p\frac{u}{\Delta_0}(\beta - \beta^\star - \alpha). \quad \text{(A7)}$$

In order to take the curvature into account we consider it as a small perturbation, which results in small deviations of the collective variables: $q = Vt + \tilde{q}$ and $\Phi = \Omega t + \tilde{\Phi}$. Substituting it in (14) and taking into account (A7) one obtains

$$\dot{\tilde{q}} = \pi v_0\kappa\ell\sqrt{1 + \frac{u^2}{v_0^2}\frac{1}{4k_t}}\cos(\Omega t + \delta_q),$$

$$\dot{\tilde{\Phi}} = \pi\omega_0\kappa\ell\sqrt{\alpha^2 k_t + \frac{1}{4}\frac{u^2}{v_0^2}(\beta - \alpha)^2}\sin(\Omega t + \delta_\Phi),$$

$$\tan\delta_q = 2\sqrt{k_t}p\frac{v_0}{u}, \quad \tan\delta_\Phi = p\frac{u}{v_0}\frac{\beta - \alpha}{\alpha}\frac{1}{2\sqrt{k_t}}.$$

Thus, the curvature adds an oscillatory component of frequency Ω to the uniform domain wall motion with velocity V. The presented analysis enables one to make an upper estimate of the frequency Ω (for the case of high current u). Therefore the condition of separation of time scales in (A3) reads $\omega \gg \Omega$, which can be also written as (13).

APPENDIX B: BIFURCATIONAL ANALYSIS OF EQUATIONS OF MOTION

Let us now make a bifurcational analysis of the system (14). Excluding $\dot{q}$ from (14) one obtains (in a low damping limit) the equation

$$\dot{\Phi} \approx \Omega\Big(1 - \frac{u_c}{u}\sin\Phi\Big). \quad \text{(B1)}$$

In mechanics, Eq. (B1) describes dynamics of an overdamped pendulum driven by a constant torque. For the case $u < |u_c|$ the equation (B1) has two fixed points, namely the stable one

$$\Phi_s = \frac{1+p}{2}\pi - p\arcsin\frac{u}{u_c}, \quad \text{(B2)}$$

see filled circles in the bifurcation diagram, Fig. 4, and the unstable one

$$\Phi_a = \frac{1-p}{2}\pi + p\arcsin\frac{u}{u_c}, \quad \text{(B3)}$$

see open circles in the bifurcation diagram, Fig. 4. In general, the criterion of stability of the fixed point $\Phi^* \in \{\Phi_s, \Phi_a\}$ reads $p\cos\Phi^* < 0$. One has only one stable fixed point, in contrast to the biaxial magnet, where two stable fixed points are present.

Let us now consider the behavior of the system at the vicinity of the bifurcation point $u = |u_c|$. As follows from (B2), $\Phi_s \to \mathrm{sgn}(\alpha - \beta + \beta^\star)\pi/2$ when $u \to |u_c|$. Introducing now small deviations $\tilde{\Phi} = \Phi - \Phi_s$ and $\tilde{u} = u - |u_c|$, one can easily obtain from (B1)

$$\Delta_0\dot{\tilde{\Phi}} = -p(\alpha - \beta + \beta^\star)(\tilde{u} + |u_c|\tilde{\Phi}^2/2). \quad \text{(B4)}$$

Relation (B4) is a normal form for a saddle-node bifurcation [44]. All possible scenarios of the bifurcation are collected in Fig. 4.

When the applied current exceeds the critical value $u > |u_c|$ the domain wall demonstrates a precession motion which is typical for the Walker limit overcoming. The period of the precession can be easily obtained by integrating (B1):

$$T = \frac{2\pi}{\Omega}\frac{1}{\sqrt{1 - u_c^2/u^2}}. \quad \text{(B5)}$$

This corresponds to the frequency (19). For the case $u \gtrapprox |u_c|$ one can estimate period (B5) as follows: $T \approx \pi\Omega^{-1}\sqrt{2|u_c|}/\sqrt{u - |u_c|}$. The obtained square-root scaling law is a very general feature of systems that are close to a saddle-node bifurcation [44].

APPENDIX C: NUMERICAL SIMULATIONS

In order to verify our analytical results we perform numerical micromagnetic simulations of the Landau-Lifshitz-Gilbert equation with additional Zhang-Li spin-torque terms

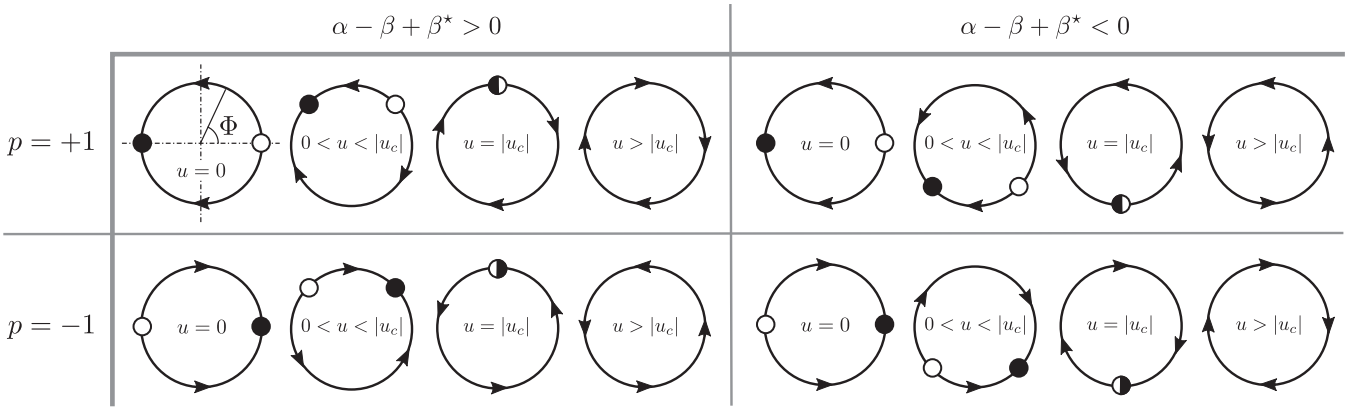

FIG. 4. All possible bifurcational diagrams for Eq. (B1) for various values of parameters. Filled and open circles show stable and unstable fixed points, respectively.

utilizing the NMAG code [40]. We restrict ourselves to the case of magnetically soft material; therefore only two magnetic interactions are taken into account, namely exchange and magnetostatic contributions.

The helix-shaped geometries are determined by (1) and (3). All the considered wires have radius $\rho_0 = 5$ nm and length $L = 6\,\mu$m [45].

Helix radius $\mathcal{R}$ and pitch $\mathcal{P}$ are determined in accordance with the required curvature and torsion

$$\mathcal{R} = \frac{\kappa}{\kappa^2 + \tau^2}, \quad \mathcal{P} = 2\pi \frac{\tau \mathcal{C}}{\kappa^2 + \tau^2}. \tag{C1}$$

In simulations we use material parameters of permalloy, namely, exchange constant $A = 1.3\,\mu$erg/cm (in SI units $A^{\mathrm{SI}} = 13$ pJ/m), saturation magnetization $M_s = 860$ G (in SI units $M_s^{\mathrm{SI}} = 860\,$kA/m), and damping coefficient $\alpha = 0.01$. These parameters result in the exchange length $\ell \approx 3.7$ nm and $\omega_0 = 30.3$ GHz. Thermal effects and anisotropy are neglected. An irregular tetrahedral mesh with cell size about 2.75 nm is used.

The numerical experiment consists of two steps. First, we use an overdamped regime ($\alpha = 0.1$) in order to relax the domain wall of the certain charge p on a helix wire with the certain geometrical parameters; see Fig. 1.

In the second step, we stimulate the motion of the domain wall by applying the spin-polarized current $\boldsymbol{u} = u\boldsymbol{e}_{\mathrm{T}}$ with natural damping coefficient $\alpha = 0.01$. For the precessional motion the time of simulation $T_{\mathrm{sim}} > 3T$ with T being the precession period. In this regime the averaged domain wall velocity is calculated as

$$\overline{V} = \frac{1}{T}\int_{t_0}^{t_0+T} \dot{q}(t)dt,$$

where the dependence $\dot{q}(t)$ is extracted from the simulations and time moment $t_0 \approx T$ is chosen not too close to the simulations beginning in order to prevent influence of possible transient processes induced by the sharp switching on the current. However, this method does not enable one to calculate $\overline{V}$ very close to the Walker limit, because of the simulation time limitation.

Typical time behavior of domain wall position $q(t)$ and phase $\Phi(t)$ is shown in Fig. 3.

[1] N. L. Schryer and L. R. Walker, The motion of 180° domain walls in uniform dc magnetic fields, J. Appl. Phys. **45**, 5406 (1974).

[2] André Thiaville and Yoshinobu Nakatani, Domain-wall dynamics in nanowires and nanostrips, in *Spin Dynamics in Confined Magnetic Structures III*, Topics in Applied Physics, Vol. 101, edited by B. Hillebrands and A. Thiaville (Springer, Berlin, 2006), pp. 161–206.

[3] A. Mougin, M. Cormier, J. P. Adam, P. J. Metaxas, and J. Ferré, Domain wall mobility, stability and Walker breakdown in magnetic nanowires, Europhys. Lett. **78**, 57007 (2007).

[4] Djemoui Bouzidi and Harry Suhl, Motion of a Bloch Domain Wall, Phys. Rev. Lett. **65**, 2587 (1990).

[5] Arseni Goussev, Ross G. Lund, J. M. Robbins, Valeriy Slastikov, and Charles Sonnenberg, Domain wall motion in magnetic nanowires: An asymptotic approach, Proc. R. Soc. A **469**, 20130308 (2013).

[6] A. Thiaville, Y. Nakatani, J. Miltat, and Y. Suzuki, Micromagnetic understanding of current-driven domain wall motion in patterned nanowires, Europhys. Lett. **69**, 990 (2005).

[7] S. Fukami, T. Suzuki, N. Ohshima, K. Nagahara, and N. Ishiwata, Micromagnetic analysis of current-driven domain wall motion in nanostrips with perpendicular magnetic anisotropy, J. Appl. Phys. **103**, 07E718 (2008).

[8] Ming Yan, Attila Kákay, Sebastian Gliga, and Riccardo Hertel, Beating the Walker Limit with Massless Domain Walls in Cylindrical Nanowires, Phys. Rev. Lett. **104**, 057201 (2010).

[9] A. Thiaville, Y. Nakatani, J. Miltat, and N. Vernier, Domain wall motion by spin-polarized current: A micromagnetic study, J. Appl. Phys. **95**, 7049 (2004).

[10] Gen Tatara and Hiroshi Kohno, Theory of Current-Driven Domain Wall Motion: Spin Transfer versus Momentum Transfer, Phys. Rev. Lett. **92**, 086601 (2004).

[11] Denis D. Sheka, Volodymyr P. Kravchuk, and Yuri Gaididei, Curvature effects in statics and dynamics of low-dimensional magnets, J. Phys. A: Math. Theor. **48**, 125202 (2015).

[12] S. Zhang and Z. Li, Roles of Nonequilibrium Conduction Electrons on the Magnetization Dynamics of Ferromagnets, Phys. Rev. Lett. **93**, 127204 (2004).

[13] At the initial moment of the current application the domain wall can demonstrate a short shift; however finally it stops and no steady motion is observed.

[14] Oleksandr V. Pylypovskyi, Denis D. Sheka, Volodymyr P. Kravchuk, Kostiantyn V. Yershov, Denys Makarov, and Yuri Gaididei, Rashba torque driven domain wall motion in magnetic helices, arXiv:1510.04725.

[15] B. Göhler, V. Hamelbeck, T. Z. Markus, M. Kettner, G. F. Hanne, Z. Vager, R. Naaman, and H. Zacharias, Spin selectivity in electron transmission through self-assembled monolayers of double-stranded DNA, Science **331**, 894 (2011).

[16] R. Naaman and David H. Waldeck, Chiral-induced spin selectivity effect, J. Phys. Chem. Lett. **3**, 2178 (2012).

[17] A. A. Eremko and V. M. Loktev, Spin-sensitive electron transmission through helical potentials, Phys. Rev. B **88**, 165409 (2013).

[18] Roberta Sessoli, Marie-Emmanuelle Boulon, Andrea Caneschi, Matteo Mannini, Lorenzo Poggini, Fabrice Wilhelm, and Andrei Rogalev, Strong magneto-chiral dichroism in a paramagnetic molecular helix observed by hard x-rays, Nat. Phys. **11**, 69 (2014).

[19] Marco Scarrozza, Alessandro Vindigni, Paolo Barone, Roberta Sessoli, and Silvia Picozzi, Combined first-principles and thermodynamic approach to m-nitronyl nitroxide (m = Co, Mn) spin helices, Phys. Rev. B **91**, 144422 (2015).

[20] Elliot J. Smith, Denys Makarov, Samuel Sanchez, Vladimir M. Fomin, and Oliver G. Schmidt, Magnetic Microhelix Coil Structures, Phys. Rev. Lett. **107**, 097204 (2011).

[21] Elliot J. Smith, Denys Makarov, and Oliver G. Schmidt, Polymer delamination: Towards unique three-dimensional microstructures, Soft Matter **7**, 11309 (2011).

[22] Ya. B. Bazaliy, B. A. Jones, and Shou-Cheng Zhang, Modification of the Landau-Lifshitz equation in the presence of a spin-polarized current in colossal- and giant-magnetoresistive materials, Phys. Rev. B **57**, R3213 (1998).

[23] Yaroslav Tserkovnyak, Arne Brataas, and Gerrit E. W. Bauer, Theory of current-driven magnetization dynamics in inhomogeneous ferromagnets, J. Magn. Magn. Mater. **320**, 1282 (2008).

[24] D. C. Ralph and M. D. Stiles, Spin transfer torques, J. Magn. Magn. Mater. **320**, 1190 (2008).

[25] Gen Tatara, Hiroshi Kohno, and Junya Shibata, Microscopic approach to current-driven domain wall dynamics, Phys. Rep. **468**, 213 (2008).

[26] Arne Brataas, Andrew D. Kent, and Hideo Ohno, Current-induced torques in magnetic materials, Nat. Mater. **11**, 372 (2012).

[27] D. G. Porter and M. J. Donahue, Velocity of transverse domain wall motion along thin, narrow strips, J. Appl. Phys. **95**, 6729 (2004).

[28] V. V. Slastikov and C. Sonnenberg, Reduced models for ferromagnetic nanowires, IMA J. Appl. Math. **77**, 220 (2012).

[29] Volodymyr P. Kravchuk, Stability of magnetic nanowires against spin-polarized current, Ukr. J. Phys. **59**, 1001 (2014).

[30] Kostiantyn V. Yershov, Volodymyr P. Kravchuk, Denis D. Sheka, and Yuri Gaididei, Curvature-induced domain wall pinning, Phys. Rev. B **92**, 104412 (2015).

[31] T. L. Gilbert, A phenomenological theory of damping in ferromagnetic materials, IEEE Trans. Magn. **40**, 3443 (2004).

[32] A. Thiaville, J. M. Garcia, and J. Miltat, Domain wall dynamics in nanowires, J. Magn. Magn. Mater. **242-245**, 1061 (2002).

[33] W. Döring, Über die trägheit der wände zwischen weißchen bezirken, Z. Naturforsch., A **3**, 373 (1948).

[34] J. C. Slonczewski, Dynamics of magnetic domain walls, Int. J. Magn. **2**, 85 (1972).

[35] A. A. Thiele, Steady-State Motion of Magnetic Domains, Phys. Rev. Lett. **30**, 230 (1973).

[36] A. P. Malozemoff and J. C. Slonzewski, *Magnetic Domain Walls in Bubble Materials* (Academic Press, New York, 1979).

[37] Volodymyr P. Kravchuk, Influence of Dzialoshinskii-Moriya interaction on static and dynamic properties of a transverse domain wall, J. Magn. Magn. Mater. **367**, 9 (2014).

[38] Denis D. Sheka, Volodymyr P. Kravchuk, Kostiantyn V. Yershov, and Yuri Gaididei, Torsion-induced effects in magnetic nanowires, Phys. Rev. B **92**, 054417 (2015).

[39] O. A. Tretiakov and Ar. Abanov, Current-Driven Magnetization Dynamics in Ferromagnetic Nanowires with a Dzyaloshinskii-Moriya Interaction, Phys. Rev. Lett. **105**, 157201 (2010).

[40] Thomas Fischbacher, Matteo Franchin, Giuliano Bordignon, and Hans Fangohr, A systematic approach to multiphysics extensions of finite-element-based micromagnetic simulations: Nmag, IEEE Trans. Magn. **43**, 2896 (2007).

[41] Eiji Saitoh, Hideki Miyajima, Takehiro Yamaoka, and Gen Tatara, Current-induced resonance and mass determination of a single magnetic domain wall, Nature (London) **432**, 203 (2004).

[42] Luc Thomas, Masamitsu Hayashi, Xin Jiang, Rai Moriya, Charles Rettner, and Stuart S. P. Parkin, Oscillatory dependence of current-driven magnetic domain wall motion on current pulse length, Nature (London) **443**, 197 (2006).

[43] See Supplemental Material at http://link.aps.org/supplemental/10.1103/PhysRevB.93.094418 for videos of steady-state and precession motions.

[44] Steven H. Strogatz, *Nonlinear Dynamics and Chaos: With Applications to Physics, Biology, Chemistry, and Engineering*, 2nd ed. (The Perseus Books Group, New York, 2014), p. 528.

[45] One can ask a natural question about the validity of the continuous phenomenological Landau-Lifshitz-Gilbert approach for thin wires. The validity of the phenomenological Landau-Lifshitz-Gilbert equations for stripe-shaped nanowires with thickness about ℓ were recently checked in Refs. [46,47] where good agreement between experimental results and predictions of phenomenological Landau-Lifshitz-Gilbert equations was found. This allows us to conclude that the use of continuous Landau-Lifshitz-Gilbert equations for our case, where the wire's thickness is $\geqslant 2\ell$, is legitimate.

[46] Satoru Emori, Uwe Bauer, Sung-Min Ahn, Eduardo Martinez, and Geoffrey S. D. Beach, Current-driven dynamics of chiral ferromagnetic domain walls, Nat. Mater. **12**, 611 (2013).

[47] Kwang-Su Ryu, Luc Thomas, See-Hun Yang, and Stuart Parkin, Chiral spin torque at magnetic domain walls, Nat. Nanotechnol. **8**, 527 (2013).